RSC Advances

PAPER

Cite this: *RSC Adv.*, 2020, **10**, 1917

Electrospun silk fibroin/TiO_2 mats. Preparation, characterization and efficiency for the photocatalytic solar treatment of pesticide polluted water

Salvador Aznar-Cervantes,[a] Marina Aliste,[b] Isabel Garrido,[b] María J. Yañez-Gascón,[c] Nuria Vela,[c] Jose L. Cenis,[a] Simón Navarro[d] and José Fenoll *[b]

Received 7th November 2019
Accepted 18th December 2019

DOI: 10.1039/c9ra09239k

rsc.li/rsc-advances

The photocatalytic properties of silk fibroin (SF) incorporating TiO_2 nanoparticles using an electrospinning technique were examined. Electrospun SF/TiO_2 mats were successfully prepared and characterized by different techniques (XRD, FE-SEM, XPS, XDS, FTIR and BET). The photocatalytic efficiency of these materials were assessed by their ability to degrade four pesticides (boscalid, hexythiazox, pyraclostrobin and trifloxystrobin) in water exposed to solar irradiation. The effect of catalyst loading on the disappearance kinetics of the different pesticides was studied in order to determine the maximum degradation efficiency. The degradation rate significantly increases upon adding the TiO_2. However, no significant differences ($p < 0.05$) were observed when the TiO_2 loading was increased from 25 to 50 mg for most compounds. Thus, SF mats with 25 mg of TiO_2 were selected. Therefore, a new and simple approach to produce materials with photocatalytic activity, safety and potential application in the purification of water contaminated by pesticides has been developed.

1 Introduction

Water pollution by organic compounds, such as pesticides, is one of the most complex environmental problems faced by researchers. Conventional biological and physical treatments of water are neither effective nor sustainable for the most recalcitrant pesticides. In this context, the development of solar photochemical technologies whereby sunlight is absorbed by a catalyst in order to change the structure of pesticides has recently aroused great interest among the scientific community for water treatment. TiO_2 nanoparticles are described in the scientific literature as efficient photocatalysts,[1] used for the degradation of a wide variety of organic pollutants due to their high activity and splendid electronic and optical properties.[2–4] In this context many attempts have been made to incorporate them into three-dimensional supports[5] that minimize the risks inherent in their systemic use for the environment and drawbacks, such as a stage of separation and recovery of TiO_2 nanoparticles.

Electrospinning is a procedure used to make micro- and nanofibrous scaffolds with uses in a diverse fields such as purification, catalysts,[6] electrical devices and biomedicine.[7–9] Silk fibroin (SF) produced by the silkworm (*Bombyx mori*) is a biocompatible[10] and natural protein that has been extensively used in recent years to produce electrospun scaffolds with a diversity of applications.[11] The structural unit of SF is composed of three elements, the heavy chain fibroin (350 kDa), the light chain fibroin (25 kDa) and protein P25, the molar proportion of these constituents is 6 : 6 : 1 respectively.[12] Additionally, SF electrospinning is commonly combined with additional functionalizing methods. Such as those involving the incorporation of molecules of interest (growth factors among others),[13] the utilization of different SF blends in combination with other polymers,[14] the adsorption of conductive polymers on its surface[15,16] or even the combination with nanoparticles designed to catalyze the degradation of chemical warfare agents.[6]

Several research groups have also combined sericulture and TiO_2 nanoparticles in works of diverse nature. In this way, some authors have even fed silkworm larvae with TiO_2 nanoparticles in different concentrations stating improvements in terms of growth, feed efficiency and silk production.[17] Other researchers have described improvements in the reproductive efficiency of *B. mori* with an increase in size, quantity and fertility of the

[a]*Biotechnology Group, Murcia Institute of Agri-Food Research and Development, C/Mayor s/n. La Alberca, 30150 Murcia, Spain*

[b]*Sustainability and Quality Group of Fruit and Vegetable Products, Murcia Institute of Agri-Food Research and Development, C/Mayor s/n. La Alberca, 30150 Murcia, Spain. E-mail: jose.fenoll@carm.es; Fax: +34 968 366 792; Tel: +34 968 366 798*

[c]*Applied Technology Group to Environmental Health, Faculty of Health Science, Catholic University of Murcia, Campus de Los Jerónimos, s/n. Guadalupe, 30107, Murcia, Spain*

[d]*Department of Agricultural Chemistry, Geology and Pedology, Faculty of Chemistry, University of Murcia, Campus Universitario de Espinardo, 30100, Murcia, Spain*

Table 1 Physical–chemical characteristics of the pesticides used in this study

Compound	MF[a]	M_W[b]	log K_{OW}[c]	VP[d]	WS[e]	GUS[f]
Boscalid	$C_{18}H_{12}Cl_2N_2O$	343.2	2.96	7.2×10^{-4}	4.6	2.66
Pyraclostrobin	$C_{19}H_{18}BrClN_3O_4$	387.8	3.99	2.6×10^{-5}	1.9	0.06
Hexythiazox	$C_{17}H_{21}ClN_2O_2S$	352.9	2.67	1.3×10^{-3}	0.5	0.03
Trifloxystrobin	$C_{20}H_{19}F_3N_2O_4$	408.4	4.50	3.4×10^{-4}	0.6	0.19

[a] Molecular formula. [b] Molecular mass (g mol^{-1}). [c] Octanol/water partition coefficient (K_{OW}). [d] Vapour pressure (mPa at 25 °C). [e] Water solubility (mg L^{-1}). [f] GUS leaching potential index.

eggs.[18] Cai *et al.*[19] also described the production of silk fibres more resistant to UV light and with reinforced mechanical properties using the same feeding technique. Furthermore, some authors have used regenerated fibroin by combining it with TiO_2 nanoparticles with different formats and applications, such as films[20] or porous scaffolds[21] for tissue engineering with improved mechanical and thermal properties. In relation to the field of electrospinning, the manufacture of silk fibroin/TiO_2 nanofibrous mats for wound dressings has also been explored, using formic acid as a solvent.[22] Another studied approach has been the electrospinning of PVA/fibroin/TiO_2 mixtures to produce a photocatalytic textile.[23] However, to the best of our knowledge, electrospun SF/TiO_2 mats have never used as photocatalyst for the removal of pesticides in water.

SF has optimal properties in terms of handling, safety and biocompatibility. Additionally, the potential manufacture of materials incorporating TiO_2 nanoparticles and SF in their composition is very promising. In this view, the aim of this work was to develop a simple, effective and innovative way to produce these kind of materials by means of electrospinning of SF dissolutions in combination with several rounds of atomization of methanolic suspensions of TiO_2 nanoparticles. In addition, the photocatalytic efficiency of these materials were also assessed by their ability to degrade four pesticides (boscalid, pyraclostrobin, hexythiazox and trifloxystrobin) in water exposed to solar irradiation.

2 Materials and methods

2.1 Insecticides and reagents

Analytical standards (boscalid, pyraclostrobin, hexythiazox and trifloxystrobin) with a purity > 99% were supplied from Dr Ehrenstorfer (Augsburg, Germany). Three commercial pesticides, Signum 26.7% w/w (boscalid) +6.7% w/w (pyraclostrobin), Jalisco 10% w/v (hexythiazox) and Flint 50% w/w (trifloxystrobin) were used for the photodegradation experiments. The main physicochemical properties of the studied insecticides are summarized in Table 1. The commercial titanium dioxide P25 (99.5%, <21 nm, 50 m^2 g^{-1}) was purchased from Nippon Aerosil Co Ltd (Osaka, Japan). Acetonitrile was purchased from Scharlau (Barcelona, Spain). A Milli-RX Water Purification System (Millipore, Bedford, MA, USA) was used to obtain deionized water.

2.2 Silk fibroin processing

Cocoons of *B. mori* were produced in the facilities of the IMIDA (Murcia, Spain). After chopping them into 4 pieces, they were boiled in 0.02 M Na_2CO_3 for 30 min, in order to perform the removal of the sericin (also known as degumming step). Then, the fresh SF was carefully washed with water and dehydrated at room temperature during 3 days. SF was subsequently dissolved using 9.3 M LiBr (Acros Organics) as a solvent for 3 h (60 °C), giving rise to a 20 wt% dissolution. Then it was dialysed against distilled water throughout 3 days (Snakeskin Dialysis Tubing 3.5 KDa MWCO, Thermo Scientific), performing eight changes of water (4 °C). The resulting 7 wt% SF dissolution was recuperated and concentrated by means of dialysis against 30 wt% PEG (11 000 Da) for 24 h, in order to reach a concentration of 20–21 wt% of SF. This dissolution was used for the electrospinning experimentations.

2.3 Electrospinning and post-treatment of SF/TiO_2 mats

The electrospinning setup utilized comprised of an isolated cabin which contained an electrically-charged needle located through a focal plate, a syringe pump, and a circular collector (metallic), whose surface (~375 cm^2) was protected using aluminium foil. The electrospinning conditions were controlled to facilitate the stabilization of the Taylor cone. The voltage applied to the capillary needle was 19–20 kV and −1.5 kV to the metallic collector. The distance between the collector and the tip of the needle was 42 cm, and the injection rate of the SF dissolution was 1 mL h^{-1}.

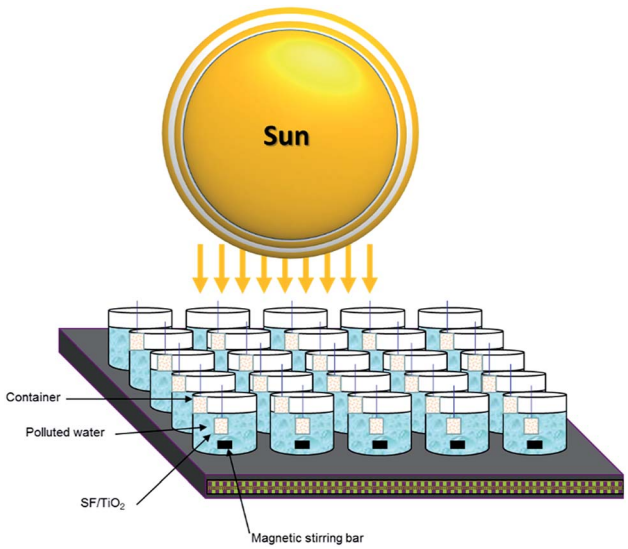

Fig. 1 Schematic drawing of the experimental setup.

Table 2 Analytical conditions of the studied pesticides

Compound	t_R (min)	SRM_1	$Fragmentor_1$ (V)	$Collision\ energy_1$ (V)	SRM_2	$Fragmentor_2$ (V)	$Collision\ energy_2$ (V)
Boscalid	25.80	343 → 307	130	20	343 → 140	130	20
Pyraclostrobin	29.20	388 → 163	90	25	388 → 194	90	10
Hexythiazox	32.70	353 → 168	110	25	353 → 228	110	15
Trifloxystrobin	30.70	409 → 186	90	15	409 → 206	90	10

The TiO_2 nanoparticles, contained in a methanolic suspension, were sprayed over the surface of the meshes during the electrospinning experiments by means of an atomizer as it is explained below.

SF mats with TiO_2 (SF/TiO_2) were produced from the electrospinning of 6 mL of 20 wt% SF dissolution. 30 mL of methanol containing 1500 mg of TiO_2 nanoparticles were sprayed during the electrospinning; 7 rounds of atomization were performed (4.3 mL per round) covering in a uniform way the whole surface of the collector. Before the first atomization and after the last one, 1.5 mL of SF dissolution were electrospun in order to produce a compact net avoiding the loss of the nanoparticles. These rounds of atomization were periodically distributed in order to guarantee the homogeneous presence of TiO_2 in the materials.

Negative controls of pure SF were produced without including nanoparticles. After production, all the electrospun mats were submitted to the annealing step performed by means of immersion in absolute methanol (30 min), in order to promote a transition of secondary structures of fibroin, increasing the β-sheet content. The mats were located among two portions of filter of paper, to ease drying and to avoid the mats from twisting. All the mats produced were gently washed with distilled water before the experiments.

2.4 X-ray diffraction (XRD), field emission scanning electron microscopy (FESEM), X-ray photoelectron spectroscopy (XPS), energy dispersive X-ray spectroscopy analysis (XDS) and surface area (SBET)

X-Ray Diffractometry (XRD), field emission scanning electron microscopy (FE-SEM), X-Ray photoelectron spectroscopy (XPS, K-ALPHA, Thermo Scientific) and energy dispersive X-ray spectroscopy analysis (EDS) were used to characterize the crystalline structure, morphology, samples surface and elemental analysis plus quantitative mapping of the photocatalysts, respectively, according to the method previously described by Garrido *et al.*[4] The nitrogen adsorption isotherms were obtained at 77 K using a Quadrasorb SI-MP by Quantachrome. Outgassing was performed with a Masterprep Degasser (Quantachrome Corp.) at 120 °C for 12 h for SF and SF/TiO_2. Specific surface areas (SSA) were determined with the Brunauer–Emmett–Teller (BET) method using the N_2 adsorption/desorption isotherm data.

2.5 Attenuated total reflectance Fourier transformed infrared spectroscopy (ATR-FTIR)

ATR-FTIR was employed with the purpose of confirming the change of SF to a non-soluble state (enriched in β-sheet structures), as well as to corroborate the presence of the nanoparticles in the materials produced, identifying the characteristic bands of TiO_2. Spectra were acquired on a Nicolet iS5 spectrometer, with an iD5 ATR accessory (Thermo Scientific, USA) using OMNIC software (Ver. 9.3.30), determining in absorbance mode with a resolution of 4 cm^{-1}, a spectral range of 4000–550 cm^{-1}, and 64 scans.

2.6 Evaluation of mechanical properties and fibre diameter of electrospun materials

A universal test frame machine (Qtest; MTS Systems, Eden Prairie, MN, USA) was used to carry out the tensile tests. The mechanical properties of the samples (10 mm × 30 mm) were proved setting a crosshead speed of 0.1 mm s^{-1} and employing a load cell of 10 N. The width of each sample was measured with a digital micrometer (Mitutoyo Digimatic Micrometer 0–25 mm, resolution of 0.001 mm and a precision of ±2 μm). The elastic modulus (MPa), tensile strength (MPa) and strain at break (%) were calculated from the resultant stress–strain curves. Elastic modulus was calculated in the linear elastic part of the curves.

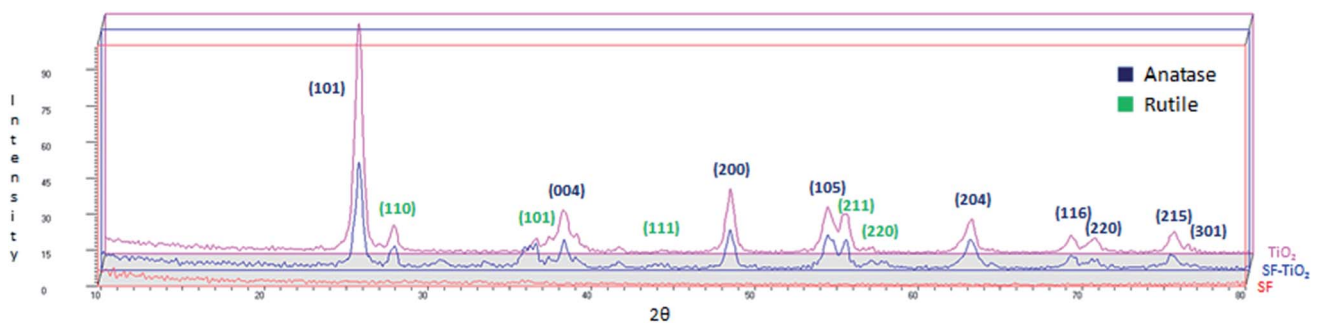

Fig. 2 XRD patterns of SF/TiO_2, SF and TiO_2.

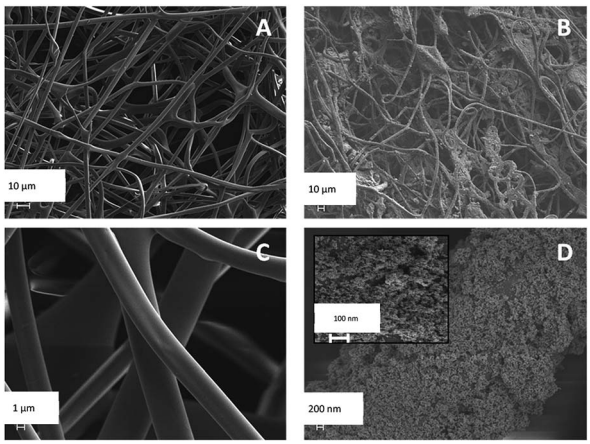

Fig. 3 SEM images of SF (A and C) and SF/TiO_2 (B and D).

Each test was accomplished at least three times per material. Additionally, SEM micrographs were used to measure the fibre diameters of the studied materials by means of image analysis (ImageJ software).

2.7 Photoreaction setup

Both trials (photocatalytic and photolytic) were carried out during August 2018, following the procedure described by Fenoll *et al.* with some modification.[24] A square fragment of SF/TiO_2 mats was introduced in each vessel containing 100 mL of water. Milli-RX water (pH 7.13, ORP 230 mV, resistivity > 5 MΩ cm (25 °C); conductivity 5.5 μS cm^{-1}, TOC < 30 μg L^{-1}; microorganisms < 10 cfu mL^{-1}) was spiked at 0.1 mg L^{-1} of each pesticide with commercial formulations and exposed to solar radiation for 180 min (from 11 AM to 2 PM). The vessels were adequately separated to avoid shielding effect. Previously to the beginning of the trials the mixture was stirred for 30 min in the dark and a sample was withdrawn to measure the dark adsorption of pesticides onto each square fragment of SF and SF/TiO_2 mats. Fig. 1 shows a schematic drawing of the experimental system used. The values (all in W m^{-2}) of VIS plus NIR, UVA and UVB at noon were 948.6 ± 52.4, 21.5 ± 2.3 and 1.7 ± 0.4, respectively.

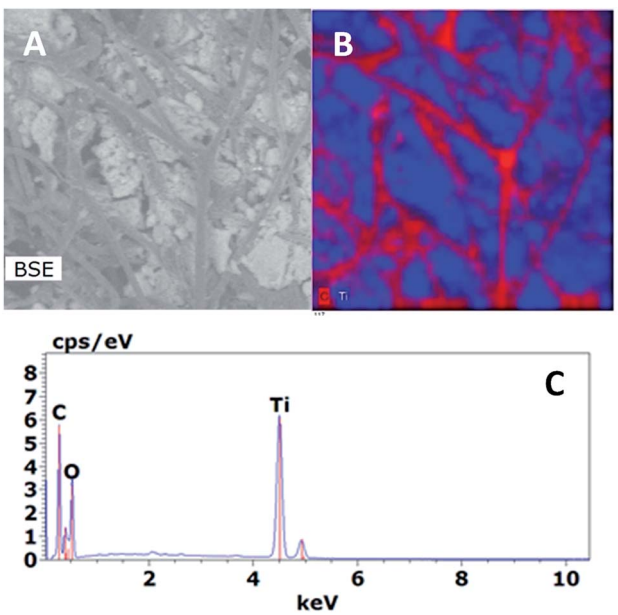

Fig. 4 Back-scattered electron (BSE) image (A), elemental mapping (B) and EDX data (C) of a SF/TiO_2 zone.

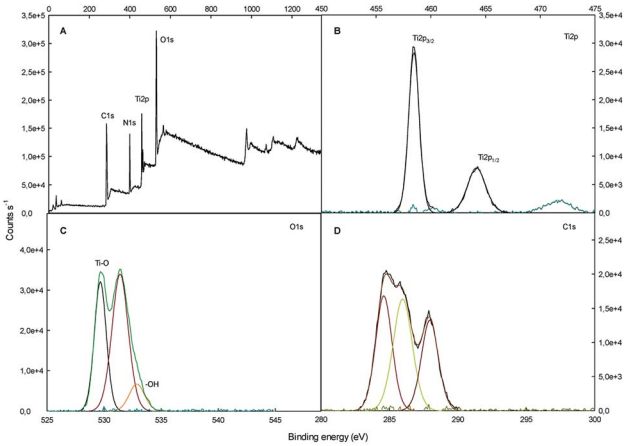

Fig. 5 XPS spectra of SF/TiO_2 sample: (A) survey spectrum, (B–D) high-resolution binding energy spectra of Ti 2p, O 1s and C 1s, respectively.

2.8 Analytical determinations

The method published by Fenoll *et al.*[25] was used to analyse pesticide residues in water samples using an HPLC system (Agilent Series 1200 Agilent Technologies, Santa Clara, CA, USA) and a G6410A triple quadrupole mass spectrometer equipped with an ESI interface operating in positive ion mode. Table 2 lists the analytical conditions of the studied pesticides. In addition, the method described by Fenoll *et al.*[24] was used to determine Ti by an Agilent 7900 ICP-MS with MicroMist glass

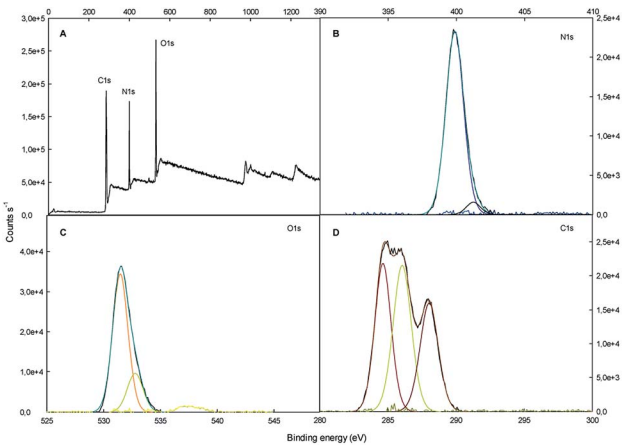

Fig. 6 XPS spectra of SF sample: (A) survey spectrum, (B–D) high-resolution binding energy spectra of N 1s, O 1s and C 1s, respectively.

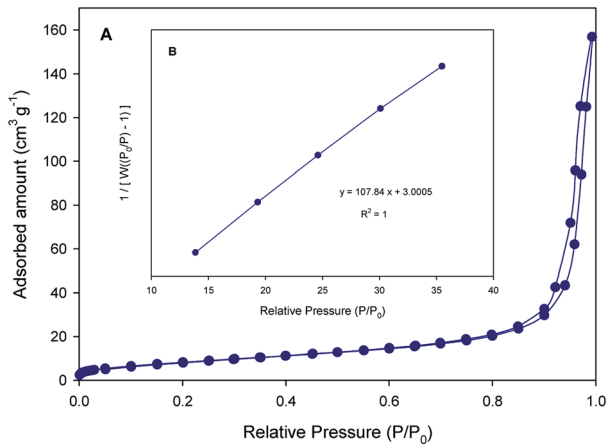

Fig. 7 (A) N_2 adsorption–desorption isotherms and (B) BET surface area plot of SF/TiO_2.

concentric nebulizer, standard nickel cones, and Ultra High Matrix Introduction (UHMI) system. Finally, the method described by Fenoll *et al.*[24] was used to measure the dissolved organic carbon (DOC) content in water samples with a Multi N/C 3100 TOC Analyzer (Analytic Jena AG, Jena, Germany) equipped with an NDIR detector (950 °C).

2.9 Statistical analysis

Curve fitting and statistical analyses was carried out using SigmaPlot version 13.0 statistical software (Systat, Software Inc., San Jose, CA). For the statistical analyses of mechanical properties and fibre diameter IBM SPSS 25 statistics software was used. Data were compared with ANOVA ($p < 0.05$) or Mann–Whitney ($p < 0.05$) tests depending if they accomplished normality and homoscedasticity requirements or not, respectively.

3 Results and discussion

3.1 Field emission scanning electron microscopy (FESEM) and X-ray diffraction (XRD)

XRD patterns of SF, SF/TiO_2 and TiO_2 P25 samples are shown in Fig. 2. No representative peaks were observed for SF. By contrast, SF/TiO_2 sample show intensive (Int/100 > 10) diffraction peaks at *ca.* 2θ of 25.3, 37.8, 48.0, 53.9, 55.1, 62.8, which corresponds to the 101, 004, 200, 105, 211, and 204 planes, all of them characteristics of anatase (ICDD PDF2 database Set-file 21-1272). For rutile phase, the higher peak (Int/100 > 10) corresponds to 2θ of 27.4 (110 plane), typical peak of rutile (ICDD PDF2 database Set-file 21-1276). Although it can be considered that the surface coverage is complete, a decrease in the overall intensity for SF/TiO_2 was observed in comparison to TiO_2 P25, which implies lower crystallinity.

The SEM images of SF and SF/TiO_2 are shown in Fig. 3. It shows a non-uniform TiO_2 layer around the SF. In addition, the SEM image of the SF/TiO_2 shows a cluster of aggregates of TiO_2 deposited on the SF with an average size of approximately 20–30 nm. Again this is consistent with the adsorption of P25 aggregates and with the data for P-25 TiO_2 provided by Degussa Co. and other researchers.[4,26,27] The elemental mapping of SF/TiO_2 showed that the surface coverage of the SF with TiO_2 was practically complete (Fig. 4).

The surface chemical composition of SF/TiO_2 and SF samples were further analyzed by XPS (Fig. 5 and 6). The survey spectrum of SF/TiO_2 and SF (Fig. 5A and 6A) shows the presence of Ti, O, N and C elements and O, N, C elements, respectively. The binding energies for the Ti $2p_{1/2}$ and Ti $2p_{3/2}$ were 464.3 and 458.4 eV, respectively, whereas in pure TiO_2 P25, these binding energies were 463.9 and 458.2 eV, respectively[4] (Fig. 5B). The O 1s spectra are also shown in Fig. 5C and 6C. The O 1s peak of SF/TiO_2 could be resolved into three peaks by the XPS peak fitting program. The presence of different oxygen species could explain the asymmetric

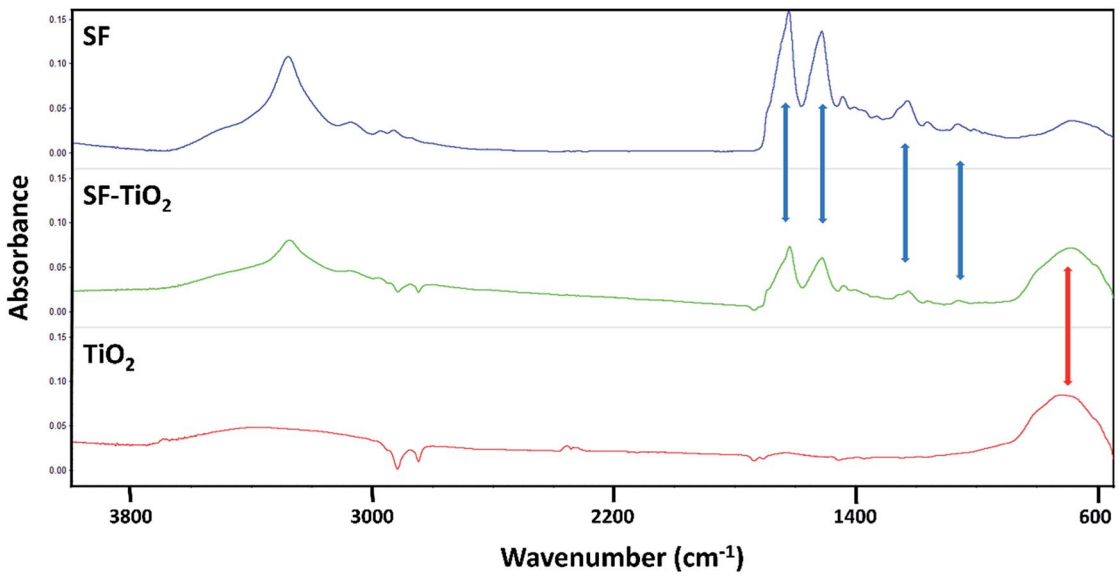

Fig. 8 Infrared spectra of pure fibroin mats (SF), mats containing TiO_2 nanoparticles (SF–TiO_2) and pure TiO_2 nanoparticles (TiO_2).

Table 3 Average values of fibre diameter and mechanical properties studied in SF and SF/TiO_2 electrospun materials

Mats	Fibre diameter (nm)	Tensile strength (MPa)	Elastic modulus (MPa)	Strain at break (%)
SF	2948 ± 748	0.409 ± 0.119	24 238 ± 8126	2278 ± 0.256
SF/TiO_2	3858 ± 1167[a]	0.331 ± 0.088	22 770 ± 5056	1848 ± 0.271

[a] Statistically different values compared to negative control (Mann–Whitney, $p < 0.05$).

nature of O 1s peaks.[28] The XPS analysis result is in accordance with the result of the XRD pattern. In addition, similar C 1s spectra are obtained for SF/TiO_2 and SF (Fig. 5D and 6D). Finally, the binding energy for the N 1s was 339.8 eV (Fig. 6B).

Gas physisorption isotherms of nitrogen or argon adsorbates are the basis to measure specific surface area (SSA) of porous material and pore size distribution.[29] In the case of SF (2 $m^2 g^{-1}$) almost no N_2 adsorption is observed, suggesting that the pore structures are very poor. Fig. 7A and B shows the N_2 adsorption/desorption isotherms and BET surface area plot of SF/TiO_2.The creation of pores and the increase of SSA in SF/TiO_2 is supported by the N_2 physisorption isotherms which show that SSA is increased to 31 $m^2 g^{-1}$, which is close to the SSA obtained for TiO_2 P25 (55 $m^2 g^{-1}$).[26]

3.2 Attenuated total reflectance Fourier transformed infrared spectroscopy (ATR-FTIR)

The results of ATR-FTIR analysis confirmed that the TiO_2 nanoparticles were incorporated effectively in the materials. Along the spectra obtained from the SF/TiO_2 meshes (Fig. 8, green line) are observed both, the characteristic bands of SF (Fig. 8, blue spectrum) and the corresponding to TiO_2 (Fig. 8, red line).

SF and SF/TiO_2 mats exhibited the peaks corresponding to amide I (1622 cm^{-1}), amide II (1515 cm^{-1}), amide III (1230 cm^{-1}) and amide IV (1064 cm^{-1}), highlighted with blue arrows in Fig. 7, these are widely described for fibroin biomaterials in β-sheet conformation.[30,31] The peak at 1660 cm^{-1} did not appear, this fact verified that the conformation of the fibroin transformed from random coil to β-sheet;[32] which implicates a transition to a non-soluble state in water. Similarly, as mentioned above, the spectra of SF/TiO_2 meshes showed a broad band at 700 cm^{-1} caused by the presence of TiO_2 in their composition (highlighted with a red arrow). This band, present also in the spectrum of pure TiO_2, is assigned to the vibrations caused due to (Ti–O–Ti) stretch.[21,33]

3.3 Mechanical properties and fibre diameters

The characterization of the mechanical properties and the diameter of the fibres of the mats produced was carried out in order to evaluate if the incorporation of the TiO_2 nanoparticles affected the properties of the fibroin materials. In the case of the diameter of the fibres, the homogeneous incorporation of a layer of TiO_2 gave rise to a statistically significant increase in their average values (Mann–Whitney, $p < 0.05$). Pure fibroin meshes presented an average value of fibre diameter of around 2.9 microns and those that included TiO_2 around 3.9 microns.

On the other hand, the values obtained for the mechanical properties were not significantly altered by the incorporation of TiO_2. These are described in Table 3 and are in the range of the ones stated in other works studying electrospun SF materials.[16,34] The tensile strength ranged between 0.3–0.4 MPa, the strain at break was estimated around 1.8–2.3% and the elastic modulus presented values between 23–24 MPa.

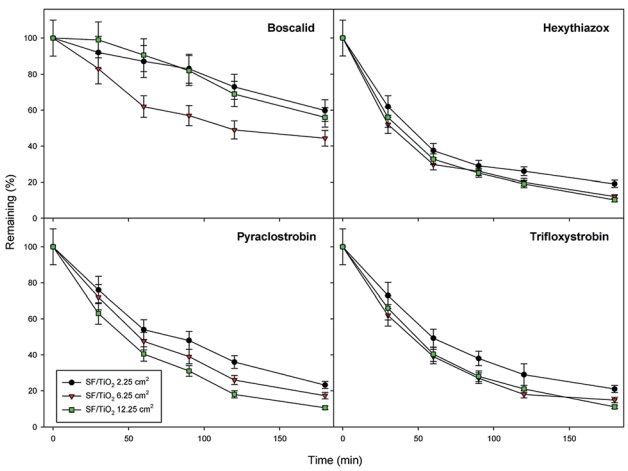

Fig. 9 Optimization of TiO_2 load for photocatalytic degradation of studied pesticides (0.1 mg L^{-1}). Error bars denote standard deviation ($n = 3$).

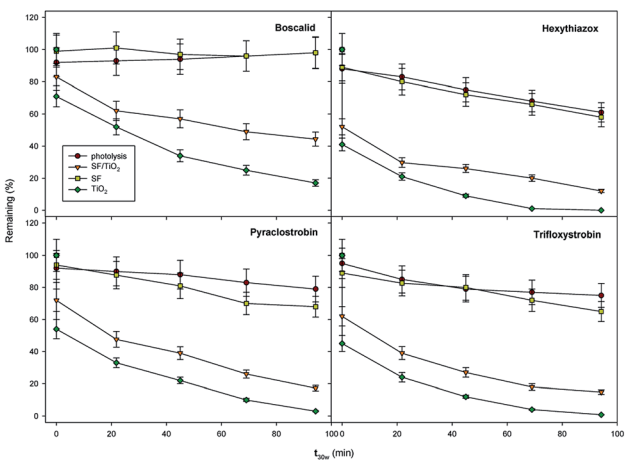

Fig. 10 Degradation kinetics in water of the studied pesticides (0.1 mg L^{-1}) by photolysis (with and without SF) and heterogeneous photocatalysis (SF/TiO_2 and TiO_2 nanopowder) during the photoperiod. Approximately 250 mg L^{-1} of TiO_2 in all cases. Error bars denote standard deviation ($n = 3$).

Table 4 Kinetic parameters for photocatalysis (SF/TiO_2 and TiO_2) of pesticides in water under natural sunlight

	SF/TiO_2			TiO_2		
Pesticide	R^2	$k \times 10^2$ (min^{-1})	$t_{\frac{1}{2}}{}^a$ (min)	R^2	$k \times 10^2$ (min^{-1})	$t_{\frac{1}{2}}{}^a$ (min)
Boscalid	0.859	0.867	79.7	0.908	1.904	36.5
Pyraclostrobin	0.897	1.836	36.7	0.827	3.217	21.5
Hexythiazox	0.731	2.506	27.6	0.759	5.287	13.1
Trifloxystrobin	0.841	2.398	28.9	0.782	4.615	15.0

[a] Referred to $t_{30\ W}$ (calculated according eqn (1)).

3.4 Photocatalytic activity and kinetics

The effect of TiO_2 loading on the disappearance kinetics of the different pesticides was evaluated in order to know maximum degradation efficiency. The experiment was carried out using three square fragments of SF/TiO_2 mats (2.25, 6.25 and 12.25 cm^2) with different TiO_2 amounts (9, 25 and 50 mg), respectively. Dark adsorption was minimal and similar for the studied insecticides on both square fragments of SF and SF/TiO_2 mats, with different size, after 30 min of incubation. The degradation rate significantly increases by adding TiO_2. However, no significant differences ($p < 0.05$) were observed when TiO_2 loading was increased from 25 to 50 mg for most compounds (except boscalid) (Fig. 9). Therefore, SF mats with 25 mg of TiO_2 were selected. The normalized illumination time ($t_{30\ W}$) was used instead of exposure time (t) to compare data from several days' and other photocatalytic experiments according to the following equation (eqn (1)).

$$t_{30\ W,\ n} = t_{30\ W,\ n-1} + \Delta t_n(\mathrm{UV}/30)(V_i/V_T)\ \Delta t_n = t_n - t_{n-1} \quad (1)$$

This equation has been used by several authors working on this topic,[35,36] where each parameter is described.

In this case, the photodegradation of boscalid, pyraclostrobin, hexythiazox and trifloxystrobin using SF/TiO_2 was evaluated (Fig. 10).

The residual levels of boscalid, pyraclostrobin, hexythiazox and trifloxystrobin after 180 min ($t_{30\ W} = 146$ min) of light exposure were 44.4, 17.3, 12.0 and 14.8 μg L^{-1}, respectively. In contrast, the photolytic decomposition of the pesticides with and without SF mats occurred at a lower rate than that observed in the photocatalytic process, and only a decrease from 58–98% of the initial concentration was achieved for hexythiazox and boscalid, respectively, after 180 min of lighting ($t_{30\ W} = 146$ min).

The dissolved organic carbon (DOC) content was measured to investigate the mineralization degree for the studied pesticides through the experiment. The initial and final content of DOC were 4.3 mg L^{-1} and 1.3 mg L^{-1}, respectively. This mineralization degree could be due to the formation of non-degradable intermediates during the solar treatment and to the presence of the coadjuvants in the commercial formulations.

The kinetic parameters of boscalid, pyraclostrobin, hexythiazox and trifloxystrobin for SF/TiO_2 and TiO_2 nanopowder are shown in Table 4. The photooxidation of the studied pesticides follows pseudo first-order behaviour consistent with the Langmuir–Hinshelwood model ($C_P = C_{P_0}\ e^{-k_{ap}t}$, where C_P is the concentration of the pesticide and k_{ap} is the apparent first-order rate constant), with R^2 values, using exposure time (t), in all cases higher than 0.938 for the four pesticides.

The rate constants for the photocatalytic oxidation of pesticides by SF/TiO_2 and TiO_2 nanopowder, using normalized illumination time ($t_{30\ W}$), varied from 0.009–0.025 and 0.019–0.053 min^{-1}, respectively. The greater S_{BET} of the TiO_2 nanopowder and the different impact and level of illumination between SF/TiO_2 and TiO_2 nanopowder could explain these differences in rate constants.[28] The smaller particle size causes larger S_{BET}. Therefore, much more space is unoccupied for the adsorption of pesticides, with the consequent improvement of the effectiveness of photocatalytic process.

The analysis of Ti into solution after the solar irradiation was carried out by ICP-MS. The presence of Ti in water during the irradiation time was found to be negligible according to previous papers.[4,26,28]

Reusability study of SF/TiO_2 was done to ensure its applicability as recycled catalyst. The photooxidation of boscalid, pyraclostrobin, hexythiazox and trifloxystrobin was performed for 720 min with sampling every 180 min (4 cycles). The decrease of rate constants for photocatalytic degradation was lower than 12% in the most unfavourable case ($n = 3$). This fact was probably due to the accumulation of organic intermediates and coadjuvants in the cavities and on the surface of the catalyst affecting the adsorption of pesticides, and reducing the activity of SF/TiO_2.

4 Conclusions

Electrospun SF/TiO_2 mats were synthesized and characterized. These materials were applied for the photocatalytic degradation of four pesticides (boscalid, hexythiazox, pyraclostrobin and trifloxystrobin) in water under sunlight. The photooxidation of these pesticides followed first order kinetics. A reusability study of SF/TiO_2 showed that the decrease of rate constants for photocatalytic degradation was lower than 12%. From the results of this work, it can be concluded that solar photocatalytic degradation using electrospun SF/TiO_2 mats can be used to remove pesticides from water in different applications. Future research should address the efficacy of the electrospun SF/TiO_2 mats with respect to other pollutants and kinds of waters.

Conflicts of interest

There are no conflicts to declare.

Acknowledgements

This work was financially supported by Operative Regional Program FEDER for Murcia 2014-2020, project RTA2015-00073-00-00, INIA 2017-2020 and with the aid of the Resolution of Presidency of State Research Agency (State Subprogram of Training of State Program of Promotion of Talent and its Employability), within the framework of the State Plan for Scientific and Technical Research and Innovation 2013-2016 co-funded by the European Social Fund. The authors are also grateful to H. Jiménez, I. Garrido, J. Cava and M. V. Molina for technical assistance. Dr Salvador D. Aznar-Cervantes acknowledges the financial support of his research contract, program INIA-CCAA (DOC INIA 2015), announced by the National Institute for Agricultural and Food Research and Technology (INIA) and supported by The Spanish State Research Agency (AEI) under the Spanish Ministry of Economy, Industry and Competitiveness.

Notes and references

1 V. Etacheri, C. Di Valentin, J. Schneider, D. Bahnemann and S. C. Pillai, *J. Photochem. Photobiol. C Photochem. Rev.*, 2015, **25**, 1–29.
2 S. Ahmed, M. G. Rasul, R. Brown and M. A. Hashib, *J. Environ. Manage.*, 2011, **92**, 311–330.
3 J. Fenoll, I. Garrido, J. Cava, P. Hellín, P. Flores and S. Navarro, *Chem. Eng. J.*, 2015, **264**, 720–727.
4 I. Garrido, M. Pastor-Belda, N. Campillo, P. Viñas, M. J. Yañez, N. Vela, S. Navarro and J. Fenoll, *J. Photochem. Photobiol., A*, 2019, **372**, 245–253.
5 K. Nakata and A. Fujishima, *J. Photochem. Photobiol. C Photochem. Rev.*, 2012, **13**, 169–189.
6 E. López-Maya, C. Montoro, L. M. Rodríguez-Albelo, S. D. Aznar Cervantes, A. A. Lozano-Pérez, J. L. Cenís, E. Barea and J. A. R. Navarro, *Angew. Chem. Int. Ed.*, 2015, **54**, 6790–6794.
7 J. Lannutti, D. Reneker, T. Ma, D. Tomasko and D. Farson, *Mater. Sci. Eng. C*, 2007, **27**, 504–509.
8 T. J. Sill and H. A. von Recum, *Biomaterials*, 2008, **29**, 1989–2006.
9 H. Liu, X. Ding, G. Zhou, P. Li, X. Wei and Y. Fan, *J. Nanomater.*, 2013, 495708, DOI: 10.1155/2013/495708.
10 Y. Wang, H. J. Kim, G. Vunjak-Novakovic and D. L. Kaplan, *Biomaterials*, 2006, **27**, 6064–6082.
11 X. Zhang, M. R. Reagan and D. L. Kaplan, *Adv. Drug Deliv. Rev.*, 2009, **61**, 988–1006.
12 S. Inoue, K. Tanaka, F. Arisaka, S. Kimura, K. Ohtomo and S. Mizuno, *J. Biol. Chem.*, 2000, **275**, 40517–40528.
13 C. Li, C. Vepari, H.-J. Jin, H. J. Kim and D. L. Kaplan, *Biomaterials*, 2006, **27**, 3115–3124.
14 J. Wang, B. Sun, M. A. Bhutto, T. Zhu, K. Yu, J. Bao, Y. Morsi, H. El-Hamshary, M. El-Newehy and X. Mo, *Front. Mater. Sci.*, 2017, **11**, 22–32.
15 S. Aznar-Cervantes, M. I. Roca, J. G. Martinez, L. Meseguer-Olmo, J. L. Cenis, J. M. Moraleda and T. F. Otero, *Bioelectrochemistry*, 2012, **85**, 36–43.
16 S. Aznar-Cervantes, A. Pagán, J. G. Martínez, A. Bernabeu-Esclapez, T. F. Otero, L. Meseguer-Olmo, J. I. Paredes and J. L. Cenis, *Mater. Sci. Eng.*, 2017, **79**, 315–325.
17 Y. Y. Li, M. Ni, F. C. Li, H. Zhang, K. Z. Xu, X. M. Zhao, J. H. Tian, J. S. Hu, B. B. Wang, W. D. Shen and B. Li, *Biol. Trace Elem. Res.*, 2016, **169**, 382–386.
18 M. Ni, F. Li, B. Wang, K. Xu, H. Zhang, J. Hu, J. Tian, W. Shen and B. Li, *Biol. Trace Elem. Res.*, 2015, **164**, 106–113.
19 L. Cai, H. Shao, X. Hu and Y. Zhang, *ACS Sustain. Chem. Eng.*, 2015, **3**, 2551–2557.
20 X.-X. Feng, L.-L. Zhang, J.-Y. Chen, Y.-H. Guo, H.-P. Zhang and C.-I. Jia, *Int. J. Biol. Macromol.*, 2007, **40**, 105–111.
21 J. H. Kim, F. A. Sheikh, H. W. Ju, H. J. Park, B. M. Moon, O. J. Lee and C. H. Park, *Int. J. Biol. Macromol.*, 2014, **68**, 158–168.
22 W. C. Jao, M. C. Yang, C. H. Lin and C. C. Hsu, *Polym. Adv. Technol.*, 2012, **23**, 1066–1076.
23 M. C. Wu, S. H. Chan and T. H. Lin, *Funct. Mater. Lett.*, 2015, **8**, 1540013.
24 J. Fenoll, I. Garrido, M. Pastor-Belda, N. Campillo, P. Viñas, M. J. Yáñez, N. Vela and S. Navarro, *Chem. Eng. J.*, 2017, **330**, 71–81.
25 J. Fenoll, P. Hellin, C. M. Martinez, P. Flores and S. Navarro, *Talanta*, 2011, **85**, 975–982.
26 J. Fenoll, I. Garrido, P. Hellin, P. Flores, N. Vela and S. Navarro, *J. Photochem. Photobiol., A*, 2015, **298**, 24–32.
27 D. Ljubas, M. Franzreb, H. C. B. Hansen and P. G. Weidler, *Sep. Purif. Technol.*, 2014, **136**, 274–285.
28 R. E. Kalan, S. Yaparatne, A. Amirbahman and C. P. Tripp, *Appl. Catal. B Environ.*, 2016, **187**, 249–258.
29 R. Bardestani, G. S. Patience and S. Kaliaguine, *Can. J. Chem. Eng.*, 2019, **97**, 2781–2891.
30 F. Zhang, B. Q. Zuo and L. Bai, *J. Mater. Sci.*, 2009, **44**, 5682–5687.
31 M. Wang, H. J. Jin, D. L. Kaplan and G. C. Rutledge, *Macromolecules*, 2004, **37**, 6856–6864.
32 H. Wang, H. Shao and X. Hu, *J. Appl. Polym. Sci.*, 2006, **101**, 961–968.
33 Y. Ochoa, Y. Ortegón, M. Vargas and J. E. Rodríguez Páez, *Rev. LatinAm. Metal. Mater.*, 2009, **1**, 931–937.
34 S. D. Aznar-Cervantes, D. Vicente-Cervantes, L. Meseguer-Olmo, J. L. Cenis and A. A. Lozano-Pérez, *Mater. Sci. Eng. C*, 2013, **33**, 1945–1950.
35 M. Hincapié, M. I. Maldonado, I. Oller, W. Gernjak, J. A. Sánchez-Pérez, M. M. Ballesteros and S. Malato, *Catal. Today*, 2005, **101**, 203–210.
36 I. Oller, W. Gernjak, M. I. Maldonado, L. A. Pérez-Estrada, J. A. Sánchez-Pérez and S. Malato, *J. Hazard. Mater.*, 2006, **B138**, 507–517.

